



A perturbation solution for bacterial growth and bioremediation in a porous medium with bio-clogging

Michael Chapwanya^{a,*}, Stephen O'Brien^b, J.F. Williams^a

^a Department of Mathematics, Simon Fraser University, Burnaby, British Columbia, Canada

^b MACSI, Department of Mathematics & Statistics, University of Limerick, Limerick, Ireland

ARTICLE INFO

Article history:

Received 25 February 2009

Received in revised form 20 October 2009

Keywords:

Porous flow

Bioremediation

Asymptotic analysis

Bio-clogging

Free boundary

ABSTRACT

We investigate a flow problem of relevance in bioremediation and develop a mathematical model for transport of contamination by groundwater and the spreading, confinement, and remediation of chemical waste. The model is based on the fluid mass and momentum balance equations and simultaneous transport and consumption of the pollutant (hydrocarbon) and nutrient (oxygen). Particular emphasis is placed on the study of processes involving the full coupling of reaction, transport and mechanical effects. Dimensional analysis and asymptotic reduction are used to simplify the governing equations, which are then solved numerically.

© 2010 Elsevier B.V. All rights reserved.

1. Introduction

Over the past few decades, numerous studies on groundwater flow have been developed with the aim of predicting the arrival times and spatial distribution of pollutants in the subsurface. The current study aims to couple groundwater flow to the model describing the degradation of pollutants in the subsurface.

We consider the transport of pollutants in a saturated phreatic aquifer below ground surface in the form of dissolved compounds or particulates in water. These pollutants percolate downward and horizontally into the aquifer due to gravity forces [1–3] and dispersion [4,5]. At this stage, there is little that can be done to control their spread and bioremediation is the cheapest remedial procedure to clean the aquifer utilizing indigenous bacteria [6]. In particular, some bioremediation procedures involve addition of nutrients to support the existing microbial activity. Examples are oxygen [7,4] and nitrate [8], which are typical factors that limit the activity of bacteria.

In the aquifers, bacterial populations grow in aqueous environments while adhering to each other and to surfaces or interfaces as biofilm [9,10] or colonies [11]. Sometimes the biofilm can cause plugging in the regions where nutrient and pollutant concentrations are high, [8,12]. As a result, laboratory tests are sometimes carried out to determine the optimal amounts of nutrients to add. Too little nutrient will result in ineffective growth rates while too much can lead to the clogging of the aquifer. For example, [13] designed an experimental nutrient addition strategy that can dampen excessive growth of bacteria at the injection point while at the same time minimising the concentration of pollutant at the end of a given period of time. Most existing mathematical models consider clogging under laboratory setups [8,14], or no bio-clogging under uniform flow velocity [15,7]. Here we wish to incorporate the processes of advection, dispersion, sorption and Monod kinetics [4,5,7,16], in the context of groundwater flow with bio-clogging under field conditions. Pore clogging is introduced by expressing biomass concentration as a nonlinear function of medium porosity [8,17].

* Corresponding address: Department of Mathematics and Statistics, Consortium for Science and Industry, University of Limerick, Limerick, Ireland.
E-mail address: mchapwan@math.sfu.ca (M. Chapwanya).

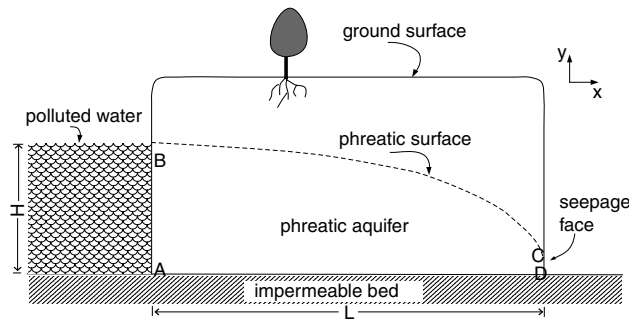


Fig. 1. Porous medium boundaries and the moving boundary of the model problem.

To obtain the pollutant advective and dispersive fluxes, we must know the fluid (i.e., the carrier) velocity. Thus we couple the biodegradation model to the necessary flow model. The flow domain, often referred to as the “dam problem”, has received considerable attention in the scientific engineering literature (cf. [18, Ch. 4], [19], [20, Ch. 13], [21]). We remark that all of these studies were aimed at finding accurate ‘steady state’ solutions for the free boundary. In the present study, the free boundary is allowed to move owing to the change in the physical properties of the porous medium.

We begin in the next section by introducing the mathematical model under investigation. The model is rendered dimensionless in Section 3 and in Section 4 we present a reduced model. An approximate solution to the reduced model is obtained in Section 4.1 using matched asymptotic expansions and later (in Section 6) we present numerical solutions to both the reduced model and the correction terms. A complete two dimensional model which includes the full coupling of reactions and flow is presented in Section 5.

2. The mathematical model

To formulate a feasible model, we assume that

1. the site has an adequate supply of nutrients, is at a suitable temperature and contains no chemicals that inhibit the biodegradation process,
2. there is no grazing of bacteria and there are no toxic substances present,
3. there is one species of bacterium, a single contaminant and a single nutrient,
4. the biofilm is treated as a continuum and all variables are described by averaging quantities such as concentrations and volume fractions,
5. the aquifer is assumed to be very long compared to the reservoir height H , $H \ll L$, we define $\delta = H/L$, where L is the horizontal length scale of the aquifer. See Fig. 1,
6. the aquifer is of sufficient extent (in the z direction in Fig. 1) that a two dimensional model is appropriate.

2.1. The flow

We consider two dimensional transport of pollutants and nutrients in a homogeneous porous medium from a polluted reservoir, Fig. 1. The domain is an aquifer with a moving boundary (phreatic surface) serving as the upper boundary and impermeable surface as the lower boundary. We assume the zone below the moving boundary is a saturated porous medium with no moisture above it.

In the saturated domain, we model flow using Darcy’s law which relates the liquid velocity $\mathbf{u}^*(u^*, v^*)$ to the pressure p^* in the following way,

$$u^* = -\frac{k^*(\theta)}{\mu_\ell \theta} \frac{\partial p^*}{\partial x^*}, \quad v^* = -\frac{k^*(\theta)}{\mu_\ell \theta} \left(\frac{\partial p^*}{\partial y^*} + \rho_\ell g \right), \tag{1}$$

where u^* and v^* are the velocity components in the x^* and y^* directions, θ is the volumetric liquid fraction, μ_ℓ is the liquid dynamic viscosity, ρ_ℓ is the liquid density, g is the acceleration due to gravity and $k^*(\theta)$ is the biomass affected permeability. The asterisk represents variables with dimensions. Conservation of the liquid requires that

$$\frac{\partial \theta}{\partial t^*} + \nabla^* \cdot (\theta \mathbf{u}^*) = 0, \tag{2}$$

assuming there are no sources and sinks within the saturated medium and that the change in density of the liquid (caused by presence of dissolved solutes) is negligible.

2.2. The biodegradation

We consider equations modeling the interaction of three quantities: the mass of substrate per unit volume of pore water s^* (g/m³), mass of nutrient per unit volume of the pore water a^* (g/m³), and mass of microbial cells per volume of the pore m^* (g/m³), see for example [17,8]. Following numerous bioremediation models in the literature (cf. [22,16,23]), the governing equations are

$$R_s \frac{\partial}{\partial t^*} (\theta s^*) = -\text{div}[\theta \mathbf{u}^* s^* - \theta \mathbf{D}^* \nabla^* s^*] - k_m \phi m^* \frac{s^*}{K_s + s^*} \frac{a^*}{K_a + a^*}, \tag{3}$$

$$\frac{\partial}{\partial t^*} (\theta a^*) = -\text{div}[\theta \mathbf{u}^* a^* - \theta \mathbf{D}^* \nabla^* a^*] - X k_m \phi m^* \frac{s^*}{K_s + s^*} \frac{a^*}{K_a + a^*}, \tag{4}$$

$$\frac{\partial m^*}{\partial t^*} = -b(m^* - m_0^*) + Y k_m m^* \frac{s^*}{K_s + s^*} \frac{a^*}{K_a + a^*}, \tag{5}$$

where R_s is the substrate retardation factor, m_0^* (g/m³) is the indigenous microbial concentration, X (g/g) is the stoichiometric constant for nutrient consumption, Y (g/g) is the yield, k_m (1/day) is the maximum rate of substrate utilization, K_a (g/m³) is the half saturation constant for nutrient a^* , K_s (g/m³) is the half saturation constant for substrate s^* , b (1/day) is the microbial decay coefficient and \mathbf{D}^* (m²/day) is a diagonal dispersion-coefficient-matrix with entries D_l^* and D_t^* corresponding to the longitudinal and transverse hydrodynamic dispersion respectively. Following [16], the retardation factor $R_s = 1 + \rho_b K_d / \theta$, where K_d (m³/g) is the distribution coefficient and ρ_b (g/m³) is the aquifer bulk density. The expression corresponds to linear equilibrium isotherm or adsorption equation.¹ Eqs. (2)–(5) are coupled by including the changes in porosity due to the growing biomass.

Note that the reaction terms in the equation involve the pointwise concentrations rather than the average concentration in a Representative Elementary Volume (REV), see [18].

In this study, we adopt the macroscopic approach [8], which makes no assumptions about the microscopic biomass distribution. A microscopic model for pore clogging will be a combination of the biofilm, microcolonies and plugs near throats. Consider a representative elementary volume U (m³/m³). Then the volumetric fraction of the liquid phase in the medium is,

$$\theta = \frac{U_\ell}{U} = \frac{U - U_s - U_m}{U} = \phi - \frac{U_m}{U} = \phi - \frac{\phi m^*}{\rho_m} = \phi \left(1 - \frac{m^*}{\rho_m} \right), \tag{6}$$

where U_ℓ , U_s and U_m are the volumes occupied by liquid phase, the solid matrix and the biomass respectively, ρ_m is the constant density of the biomass. We use $\phi = 1 - \theta_s$ to denote the constant medium porosity neglecting the presence of the biomass. Thus (6) relates the change in biomass concentration to medium porosity. The expression assumes the solid phase can be separated into volume occupied by biomass and volume occupied by the soil matrix with all the biomass responsible for degradation attached to the soil matrix.

We close this system using an expression relating the liquid fraction to the porous media permeability. Following [17], we write

$$k^*(\theta) = k^*(\phi) \left(\frac{\theta}{\phi} \right)^{19/6},$$

where $k^*(\phi)$ is the medium permeability in the absence of biomass. We define $k^*(\phi) = k_0 = \text{constant}$, which is consistent with a nondeformable saturated porous media in the absence of biomass.

2.3. Boundary and initial conditions

We need boundary conditions to solve Eq. (2) in the saturated domain. On the solid impermeable surface $\mathbf{u}^* \cdot \hat{\mathbf{n}} = 0$, i.e., the normal velocity is zero. At the Earth’s surface or the saturation level in the ground the pressure can be taken as zero i.e., $p^* = 0$ after subtracting off atmospheric pressure. A moving boundary occurs where we have an interface between a liquid and a gas. We ignore flow in the unsaturated region so that the moving boundary position is given by the kinematic condition and water flows between the impermeable surface and the moving surface at $y^* = h^*(x^*, t^*)$. We therefore need to solve the flow equations subject to the following boundary conditions

$$v^* = 0 \quad \text{on } y^* = 0,$$

¹ Isotherms are adsorption relations between the liquid phase concentration, say C and sorbed phase concentration, say \bar{C} . The semi-empirical relation to represent the equilibrium sorption in [24], is given by $\bar{C} = K_d C^n$ where K_d is the distribution coefficient and n is the Freundlich exponent. If $n = 1$, the Freundlich isotherm reduces to the linear isotherm.

$$\begin{aligned}
 p^* &= 0, & v^* &= \frac{\partial h^*}{\partial t^*} + u^* \frac{\partial h^*}{\partial x^*} \quad \text{on } y^* = h^*(x^*, t^*), \\
 p^* &= \rho_\ell g(H - y^*) \quad \text{on } x^* = 0, \\
 p^* &= 0 \quad \text{on } x^* = L.
 \end{aligned}$$

The last condition assumes no ponding (i.e., no body of water exists) at the seepage face so that the boundary is at atmospheric pressure.

We consider a bioremediation model where the porous medium is assumed to have an average nutrient inflow concentration a_0 at $x^* = 0$ and constant background concentration of the biomass m_0 . The substrate leaks through the saturated porous media from the left reservoir to the right at an average concentration s_0 , (see Fig. 1). Thus along the side AB , there is continuity of the pollutant and nutrient flux. The boundary is assumed to be stationary so that

$$[\mathbf{u}^*(c_0 - c^*) + \mathbf{D}^* \nabla c^*] \cdot \hat{\mathbf{n}} = 0,$$

where c^* denotes the concentration of either the nutrient or the substrate.

Along AD , the surface is impervious to flow of both the pollutant and the nutrient so that the normal velocity is zero. The boundary condition for substrate and nutrient is $(\nabla c^*) \cdot \hat{\mathbf{n}} = 0$.

Along CD , there is a seepage face. Polluted water emerges from the porous medium into the environment and no porous medium exists on the external side. At this outflow boundary, we have a continuity of the diffusive flux across the boundary so that $(\nabla c^*) \cdot \hat{\mathbf{n}} = 0$ for both the substrate and the nutrient.

Along the phreatic surface BC , i.e., $y = h^*(x^*, t^*)$, there is an interface between two fluids. Below the interface there is a saturated porous medium and the region below is assumed to be unsaturated (occupied by air). The boundary is stationary and there is no diffusive flux normal to the surface. The boundary condition along this surface is $(\mathbf{D}^* \nabla c^*) \cdot \hat{\mathbf{n}} = 0$.

The initial conditions assume a pollutant and nutrient free (after subtracting off the background concentration) porous media with a background biomass concentration m_0 .

3. Non-dimensionalisation

The system of equations is rendered dimensionless by introducing the following scaled variables

$$\begin{aligned}
 x &= \frac{x^*}{L}, & y &= \frac{y^*}{H}, & p &= \frac{p^*}{\rho_\ell gH}, & u &= \frac{u^* \mu_\ell L}{k_0 \rho_\ell gH}, & v &= \frac{v^* \mu_\ell}{k_0 \rho_\ell g}, \\
 t &= \frac{t^* k_0 \rho_\ell gH}{\mu_\ell L^2}, & k &= \frac{k^*}{k_0}, & s &= \frac{s^*}{s_0}, & a &= \frac{a^*}{a_0}, & m &= \frac{m^*}{m_0}.
 \end{aligned} \tag{7}$$

In addition, we also scale θ with ϕ . The dimensionless equation governing the liquid flow is

$$\delta^2 \frac{\partial \theta}{\partial t} = \delta^2 \frac{\partial}{\partial x} \left(k(\theta) \frac{\partial p}{\partial x} \right) + \frac{\partial}{\partial y} \left(k(\theta) \left[\frac{\partial p}{\partial y} + 1 \right] \right), \tag{8}$$

with the following boundary conditions

$$\begin{aligned}
 \frac{\partial p}{\partial y} &= -1 \quad \text{on } y = 0, \\
 p &= 0, & \delta^2 \frac{\partial h}{\partial t} &= - \left(k(\theta) \left[\frac{\partial p}{\partial y} + 1 \right] \right) + \delta^2 k(\theta) \frac{\partial p}{\partial x} \frac{\partial h}{\partial x} \quad \text{on } y = h, \\
 p &= (1 - y) \quad \text{on } x = 0, \\
 p &= 0 \quad \text{on } x = 1,
 \end{aligned}$$

where $k(\theta) = (1 - m\chi)^{19/6}$ and $\chi = m_0/\rho_m$. The ratio χ is a measure of the effects of biomass growth on medium porosity. A small value of χ implies that the initial biomass mass per unit volume of the porous medium is very small so that it has no effect on medium porosity and permeability.

The dimensionless biodegradation equations are

$$R_s \frac{\partial}{\partial t} (\theta s) = -\nabla \cdot \mathbf{u} \theta s + \text{div}(\theta \mathbf{D} \nabla s) - \lambda_1 m \frac{s}{\kappa_s + s} \frac{a}{\kappa_a + a}, \tag{9}$$

$$\frac{\partial}{\partial t} (\theta a) = -\nabla \cdot \mathbf{u} \theta a + \text{div}(\theta \mathbf{D} \nabla a) - \lambda_1 \lambda_2 m \frac{s}{\kappa_s + s} \frac{a}{\kappa_a + a}, \tag{10}$$

$$\frac{\partial m}{\partial t} = -\lambda_1 \lambda_4 (m - 1) + \lambda_1 \lambda_3 m \frac{s}{\kappa_s + s} \frac{a}{\kappa_a + a}, \tag{11}$$

where $\mathbf{u} = (u, v/\delta^2)$ is the velocity, $R_s = 1 + A/\theta$ is the substrate retardation factor (A is a constant), $\mathbf{D} = \text{diag}(\varepsilon_l, \varepsilon_t/\delta^2)$ is a diagonal matrix, $\kappa_s = K_s/s_0$ and $\kappa_a = K_a/a_0$. The dimensionless parameters are

$$\lambda_1 = \frac{m_0 \mu_\ell L^2}{s_0 k_0 \rho_\ell g H} k_m, \quad \lambda_2 = X, \quad \lambda_3 = \frac{s_0 Y}{m_0}, \quad \lambda_4 = \frac{s_0 b}{m_0 k_m}, \quad Pe_l = \frac{k_0 \rho_\ell g H}{\mu_\ell D_l}, \quad Pe_t = \frac{k_0 \rho_\ell g H}{\mu_\ell D_t} \tag{12}$$

and we will write $\varepsilon_l = 1/Pe_l$ and $\varepsilon_t = 1/Pe_t$.

The corresponding boundary conditions are as follows: along $x = 0$ we have

$$\varepsilon_l \frac{\partial s}{\partial x} = u(s - 1), \quad \varepsilon_l \frac{\partial a}{\partial x} = u(a - 1),$$

along the moving boundary $y = h(x, t)$ we have

$$-\varepsilon_l \frac{\partial h}{\partial x} \frac{\partial s}{\partial x} + \frac{\varepsilon_t}{\delta^2} \frac{\partial s}{\partial y} = 0, \quad -\varepsilon_l \frac{\partial h}{\partial x} \frac{\partial a}{\partial x} + \frac{\varepsilon_t}{\delta^2} \frac{\partial a}{\partial y} = 0,$$

along the seepage face $x = 1$, we have

$$\frac{\partial s}{\partial x} = 0, \quad \frac{\partial a}{\partial x} = 0,$$

and along the impermeable surface $y = 0$, we have

$$\frac{\partial s}{\partial x} = 0, \quad \frac{\partial a}{\partial x} = 0.$$

In Section 5, we consider some solutions of these two dimensional equations. In the next section we present both numerical and approximate analytical solutions to the reduced one dimensional equations in the limit of $\chi \ll 1, \delta^2 \ll 1$ and $\varepsilon_\ell \ll 1$.

4. The reduced model

To make some analytic progress, and as one issue of relevance is an estimate of the time taken for the pollutants to travel through the aquifer, we will first seek approximate one dimensional solutions in the spirit of shallow water waves [25] (with $c \approx c(x, t)$) based on the smallness of δ . These solutions would be appropriate for the case of small aspect ratio, where the boundary condition at $x = 0$ is approximately constant or where the vertical Peclet number is large enough to make the concentration approximately one dimensional [26]. We thus assume that $c \approx c(x, t)$, $a \approx a(x, t)$ and $m \approx m(x, t)$ which satisfies the boundary conditions.

4.1. Approximate one dimensional equations

In the first instance we will neglect the effect of pore clogging and take $\chi \equiv 0$. Thus we will assume that the medium permeability $k = 1$, the retardation factor $R_s \approx \hat{R}_s = 1 + A = \text{constant}$ and the porosity $\theta = 1$. The flow is governed by the equation

$$\delta^2 \frac{\partial^2 \hat{p}}{\partial x^2} + \frac{\partial^2 \hat{p}}{\partial y^2} = 0, \tag{13}$$

with the following boundary conditions

$$\frac{\partial \hat{p}}{\partial y} = -1 \quad \text{on } y = 0, \tag{14}$$

$$\hat{p} = 0, \quad \delta^2 \frac{\partial \hat{h}}{\partial t} = - \left[\frac{\partial \hat{p}}{\partial y} + 1 \right] + \delta^2 \frac{\partial \hat{p}}{\partial x} \frac{\partial \hat{h}}{\partial x} \quad \text{on } y = \hat{h}(x, t),$$

$$\hat{p} = (1 - y) \quad \text{on } x = 0,$$

$$\hat{p} = 0 \quad \text{on } x = 1.$$

The corresponding reduced bioremediation equations (after applying the mass conservation equation) are

$$\hat{R}_s \frac{\partial \hat{s}}{\partial t} = -\hat{u} \frac{\partial \hat{s}}{\partial x} + \varepsilon_l \frac{\partial^2 \hat{s}}{\partial x^2} - \lambda_1 \hat{m} \frac{\hat{s}}{\kappa_s + \hat{s}} \frac{\hat{a}}{\kappa_a + \hat{a}}, \tag{15}$$

$$\frac{\partial \hat{a}}{\partial t} = -\hat{u} \frac{\partial \hat{a}}{\partial x} + \varepsilon_l \frac{\partial^2 \hat{a}}{\partial x^2} - \lambda_1 \lambda_2 \hat{m} \frac{\hat{s}}{\kappa_s + \hat{s}} \frac{\hat{a}}{\kappa_a + \hat{a}}, \tag{16}$$

$$\frac{\partial \hat{m}}{\partial t} = -\lambda_1 \lambda_4 (\hat{m} - 1) + \lambda_1 \lambda_3 \hat{m} \frac{\hat{s}}{\kappa_s + \hat{s}} \frac{\hat{a}}{\kappa_a + \hat{a}}. \tag{17}$$

The boundary conditions are as follows: at $x = 0$ we have

$$\varepsilon_l \frac{\partial \hat{s}}{\partial x}(0, t) = \hat{u}(0, t)[\hat{s}(0, t) - 1], \quad \varepsilon_l \frac{\partial \hat{a}}{\partial x}(0, t) = \hat{u}(0, t)[\hat{a}(0, t) - 1], \quad (18)$$

and at $x = 1$ we have

$$\frac{\partial \hat{s}}{\partial x}(1, t) = 0 \quad \text{and} \quad \frac{\partial \hat{a}}{\partial x}(1, t) = 0. \quad (19)$$

The initial conditions are

$$\hat{s}(x, 0) = 0, \quad \hat{a}(x, 0) = 0, \quad \hat{m}(x, 0) = 1. \quad (20)$$

It will be shown later how, at leading order, the flow model is reduced to finding the moving boundary position only. The reduced perturbation model can be solved in two stages: solving for the steady state flow velocity and then using the result in the biodegradation equations. In fact, the leading order approximation reduces the model from a moving boundary problem to a free boundary problem.

4.1.1. Solution to the reduced flow problem

Considering the equations above, we choose a distinguished limit $\delta^2 = \sqrt{\varepsilon_l}$ and seek solutions of the form

$$\hat{p} = \psi_0 + \sqrt{\varepsilon_l} \psi_1 + \mathcal{O}(\sqrt{\varepsilon_l}^2), \quad \text{and} \quad \hat{h} = f_0 + \sqrt{\varepsilon_l} f_1 + \mathcal{O}(\sqrt{\varepsilon_l}^2). \quad (21)$$

Substituting Eqs. (21) into (13), at leading order we have

$$\frac{\partial^2 \psi_0}{\partial y^2} = 0,$$

which, together with the boundary conditions, can be solved to give

$$\psi_0 = f_0 - y. \quad (22)$$

At the next order we obtain:

$$\frac{\partial^2 \psi_1}{\partial y^2} = -\frac{\partial^2 f_0}{\partial x^2}, \quad \text{for} \quad \frac{\partial \psi_1}{\partial y} = 0 \text{ on } y = 0,$$

which reduces to

$$\frac{\partial \psi_1}{\partial y} = -y \frac{\partial^2 f_0}{\partial x^2}. \quad (23)$$

Note that Eqs. (22)–(23) can be combined to give the Dupuit–Forchheimer equation, i.e.,

$$\frac{\partial f_0}{\partial t} = \frac{\partial}{\partial x} \left(f_0 \frac{\partial f_0}{\partial x} \right), \quad (24)$$

with left side boundary condition $f_0(0, t) = 0$. It is not obvious what boundary condition to use on the seepage face since from Eq. (22) we require that $f_0(1, t) = y$. This will be overcome by obtaining a numerical solution to the full problem. However, from expressions (22) and (23) it can be deduced that the flow velocity is given by

$$\hat{u} \approx -\frac{\partial f_0}{\partial x}, \quad \hat{v} \approx \sqrt{\varepsilon_l} y \frac{\partial^2 f_0}{\partial x^2}, \quad (25)$$

which are the expressions that relate flow velocity to the free surface. From a numerical point of view we only need to solve the flow problem once in order to obtain a solution to the reduced model. In particular, we have to find the position of the free boundary $y = f_0(x)$.

The flow problem can be solved by the Dupuit assumptions based on the approximation that the aquifer is long and thin as outlined in [20], in which case the flow is essentially in the horizontal direction. In the case of phreatic flow, the phreatic surface always terminates at a point above the water table of the body of open water present outside the flow domain. This region (CD in Fig. 1), is known as the seepage face. The approximation in [20] does not apply in regions where vertical flow cannot be neglected such as at the seepage face. Using this approximation, the free surface can be found to be $f_0 = (1-x)^{1/2}$. In fact the velocity profile will be found to be infinite at $x = 1$ using Eq. (25). However, it can be shown that

$$f_0 = \sqrt{1 - vx},$$

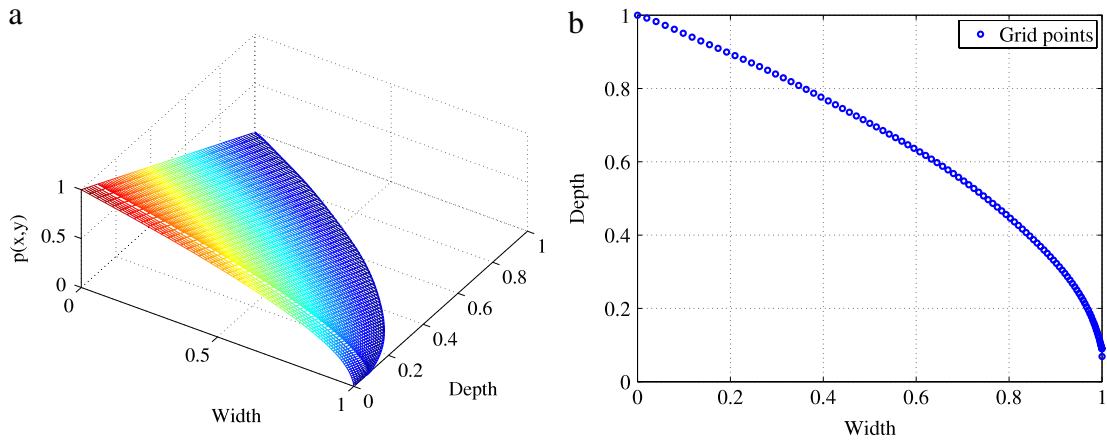


Fig. 2. (a) Pressure profile computed for $\sqrt{\epsilon_1} = 0.05$. (b) Grid used to resolve the seepage face. Note the mesh refinement towards the seepage face.

4.1.2. Computing the exact position of the free boundary

The flow equations are discretized in space at node (i, j) using a centered finite difference approximation. The discretized finite difference approximations are substituted into the governing equations to give a set of algebraic equations that are solved using the SOR (Successive Over Relaxation) method. In particular, we discretize the medium so that the nodes always terminate on the free boundary (see [27]). A variable grid is used in all directions.

4.1.3. Numerical strategy

1. Choose an initial guess for the surface $y = \hat{h}_i(x)$, and solve (8) in the region Ω enclosed by $0 \leq x \leq 1$ and the free surface $y = \hat{h}_i(x)$. The boundary conditions are given in (14).
2. Find the pressure $\hat{p}_r = \hat{p}(x, y = \hat{h}_i(x))$, i.e., pressure on the grid points along the free boundary.
3. If the pressure $\hat{p}_r = 0$, stop: then the phreatic surface is given by $y = \hat{h}_i(x)$, otherwise go to step (4).
4. If $|\hat{p}_r(x, \hat{h}_i(x))| > \Delta$, where Δ is a small positive number, move the points on the free boundary according to

$$\hat{h}_{i+1} = \hat{h}_i + C\hat{p}_r(x, \hat{h}_i(x)),$$

where C is a positive constant; then go to (2) and repeat with a new and better approximation $y = \hat{h}_{i+1}(x)$.

The pressure is positive inside the saturated region and negative outside it.² Thus steps (3) and (4) in the numerical algorithm depend on whether the point is inside or outside the saturated region. At the free boundary we have two boundary conditions, see Eqs. (14). Thus our numerical algorithm has to satisfy the two conditions simultaneously. The iterative process involves solving for \hat{p} in a region with fixed boundaries at every stage.

To resolve the seepage face accurately and efficiently we have used a non-uniform grid. Given that the height of the face is not known in advance, we have constructed a grid based on the interface when there is no seepage face, i.e., $h(x) = \sqrt{1 - x}$. This is the most singular situation and so provides a suitable grid in the general case. We simply take a uniform partition in the y direction and map that into the x direction, that is, we uniformly discretize y and then solve for x via $y = \sqrt{1 - x}$. This procedure gives $x_i = (1 - (i/N - 1)^2)$, where there are N grid points on the interval $[0, 1]$, and defines a geometric grid with excellent resolution near the seepage face, see Fig. 2.

The resulting phreatic surface is given in Fig. 3(a). In particular, we fitted the approximate solution $\hat{h} = \sqrt{1 - \nu x}$ to the numerical solution. The best fit gave $\nu = 0.992$. In the figure, we also give a comparison of the approximate solution $\hat{h} = (1 - x)^{1/2}$, [20, Ch. 13] (no seepage face) and the fitted numerical result. Fig. 2(a) gives the pressure profile for the case with a seepage face, and Fig. 3(b) gives the relationship between horizontal distance and velocity in the x direction. If we had used the boundary condition $\hat{h}(1, t) = 0$, then the free surface would be perpendicular to the x -axis at $x = 1$. In fact using (25), the horizontal velocity using (25) is $\hat{u} \approx -\frac{1}{2}(1 - x)^{-1/2}$ which is infinite at $x = 1$.

4.1.4. Approximate solution to the reduced biodegradation equations

In this section we will consider the method of matched asymptotic expansions to obtain an approximate solution to the biodegradation equations. The initial conditions assume a pollutant and nutrient free porous medium and constant indigenous biomass concentration $\hat{m} = 1$. The boundary and initial conditions are given in (18)–(20).

² In partially saturated regions, water is held under surface tension adhering to the porous media grains and any flow occurs (between grains) through micropores. The surface tension provides a pressure less than atmospheric. But atmospheric pressure is used as datum to measure soil water pressure, thus values less than atmospheric are at negative pressure (or tension).

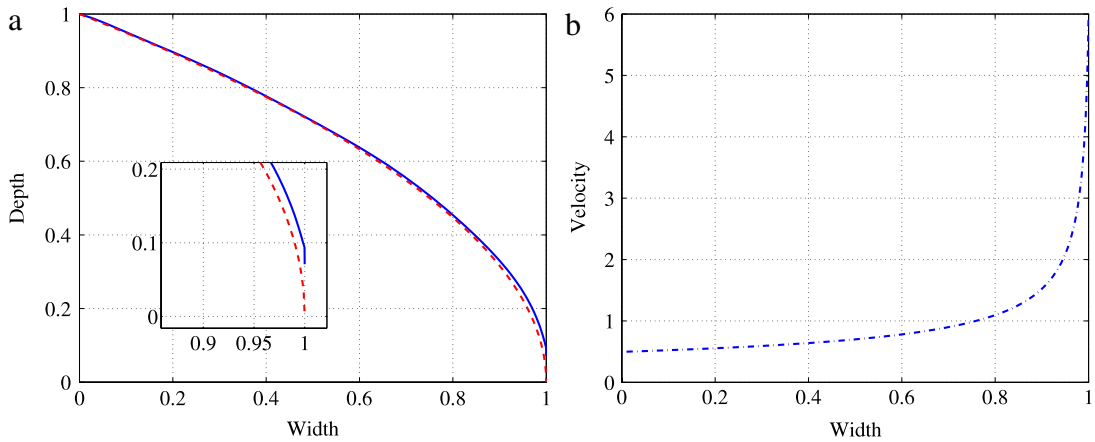


Fig. 3. (a) Comparison of the approximate solution and the numerical solution. The broken line is the approximate solution and the solid line is the fitted numerical solution. The approximate solution is given by $\hat{h} = (1 - x)^{1/2}$ and $\sqrt{\varepsilon_l} = 0.051$. Height of seepage face is 0.0920. (b) Longitudinal velocity with dimensionless distance.

4.1.5. Outer solution

Consider the dimensionless governing equations given in (15)–(17) in the limit of large Peclet number, $\varepsilon_l \ll 1$. We choose a distinguished limit $\lambda_1 = \alpha\sqrt{\varepsilon_l}$, $\alpha = \mathcal{O}(1)$, so the governing equations reduce to

$$\hat{R}_s \frac{\partial \hat{s}}{\partial t} = -\hat{u} \frac{\partial \hat{s}}{\partial x} - \alpha\sqrt{\varepsilon_l} \hat{m} \frac{\hat{s}}{\kappa_s + \hat{s} \kappa_a + \hat{a}}, \tag{26}$$

$$\frac{\partial \hat{a}}{\partial t} = -\hat{u} \frac{\partial \hat{a}}{\partial x} - \alpha\lambda_2 \sqrt{\varepsilon_l} \hat{m} \frac{\hat{s}}{\kappa_s + \hat{s} \kappa_a + \hat{a}}, \tag{27}$$

$$\frac{\partial \hat{m}}{\partial t} = -\alpha\lambda_4 \sqrt{\varepsilon_l} (\hat{m} - 1) + \alpha\lambda_3 \sqrt{\varepsilon_l} \hat{m} \frac{\hat{s}}{\kappa_s + \hat{s} \kappa_a + \hat{a}}, \tag{28}$$

with boundary conditions

$$\hat{s}(0, t) = 1, \quad \hat{a}(0, t) = 1, \quad \frac{\partial \hat{s}}{\partial x}(1, t) = 0, \quad \frac{\partial \hat{a}}{\partial x}(1, t) = 0,$$

and initial conditions

$$\hat{s}(x, 0) = 0, \quad \hat{a}(x, 0) = 0, \quad \hat{m}(x, 0) = 1.$$

In Eq. (26), the initial and boundary conditions introduce a discontinuity or shock moving at speed $s'(t)$ satisfying

$$\xi'_s(t) = \frac{[\hat{u}\hat{s}]_-^+}{[\hat{R}_s\hat{s}]_-^+}, \tag{29}$$

where the square brackets represents a jump in the enclosed quantity between its value on the left side (–) and the right side (+) of the shock. The shock position is given by $\xi_s(t) = \frac{\hat{u}_- t}{\hat{R}_s}$ satisfying the initial condition $\xi_s(0) = 0$. For simplicity we will use $\hat{u} = \hat{u}_- = \text{constant}$ in the approximate solution. Computing the outer solution up to $\mathcal{O}(\sqrt{\varepsilon_l})$ terms, we obtain

$$\hat{s}(x, t) = \begin{cases} 1 - \sqrt{\varepsilon_l} \frac{\alpha x}{\hat{u}_-} \frac{1}{\kappa_a + 1} \frac{1}{\kappa_s + 1}, & 0 \leq x \leq \hat{u}_- t / \hat{R}_s; \\ 0, & x > \hat{u}_- t / \hat{R}_s, \end{cases}$$

$$\hat{a}(x, t) = \begin{cases} 1 - \sqrt{\varepsilon_l} \frac{\alpha \lambda_2 x}{\hat{u}_-} \frac{1}{\kappa_a + 1} \frac{1}{\kappa_s + 1}, & 0 \leq x \leq \hat{u}_- t / \hat{R}_s; \\ 1, & \hat{u}_- t / \hat{R}_s \leq x \leq \hat{u}_- t; \\ 0, & x > \hat{u}_- t, \end{cases}$$

$$\hat{m}(x, t) = \begin{cases} 1 + \alpha \lambda_3 \sqrt{\varepsilon_l} \frac{1}{\kappa_a + 1} \frac{1}{\kappa_s + 1} t, & 0 \leq x \leq \hat{u}_- t / \hat{R}_s; \\ 0, & x > \hat{u}_- t / \hat{R}_s, \end{cases}$$

for $\lambda_1 = \alpha\sqrt{\varepsilon_l}$. Here we observe that the effects of the reaction terms occur in the $\mathcal{O}(\sqrt{\varepsilon_l})$ terms.

4.1.6. Inner solution

Consider Eq. (15) governing the substrate concentration, i.e.,

$$\hat{R}_s \frac{\partial \hat{s}}{\partial t} = -\hat{u} \frac{\partial \hat{s}}{\partial x} + \varepsilon_l \frac{\partial^2 \hat{s}}{\partial x^2} - \alpha \sqrt{\varepsilon_l} \hat{m} \frac{\hat{s}}{\kappa_s + \hat{s}} \frac{\hat{a}}{\kappa_a + \hat{a}}. \tag{30}$$

We introduce the interior-layer coordinates $\bar{x} = [x - \xi_s(t)]/\varepsilon_l^n$ and $t = \tau$ where $\xi_s(\tau)$ is a single (smooth) curve across which the outer solution is discontinuous. We also use $\hat{s}(x, t) = c(\bar{x}, \tau)$, $\hat{a}(x, t) = g(\bar{x}, \tau)$ and $\hat{m}(x, t) = \eta(\bar{x}, \tau)$ to denote the solution in this layer. Balancing terms requires $n = 1/2$, so we have

$$\hat{R}_s \frac{\partial c}{\partial \tau} - \hat{R}_s \frac{\xi'_s(\tau)}{\sqrt{\varepsilon_l}} \frac{\partial c}{\partial \bar{x}} = -\frac{\hat{u}_-}{\sqrt{\varepsilon_l}} \frac{\partial c}{\partial \bar{x}} + \frac{\partial^2 c}{\partial \bar{x}^2} - \alpha \sqrt{\varepsilon_l} \eta \frac{c}{\phi \kappa_s + c} \frac{g}{\phi \kappa_a + g}, \tag{31}$$

on $\bar{x} \in (-\infty, \infty)$. The boundary conditions come from matching with the outer solution. That is

$$c \rightarrow \mathcal{A}_s, \text{ as } \bar{x} \rightarrow -\infty \text{ and } c \rightarrow 0, \text{ as } \bar{x} \rightarrow +\infty, \tag{32}$$

where $\mathcal{A}_s = 1 - \sqrt{\varepsilon_l} \frac{\alpha \lambda}{\hat{u}_- \kappa_a + 1} \frac{1}{\kappa_s + 1}$. We assume that $c(\bar{x}, \tau) = c_0(\bar{x}, \tau) + \mathcal{O}(\sqrt{\varepsilon_l})$, $g(\bar{x}, \tau) = g_0(\bar{x}, \tau) + \mathcal{O}(\sqrt{\varepsilon_l})$ and $\eta(\bar{x}, \tau) = \eta_0(\bar{x}, \tau) + \mathcal{O}(\sqrt{\varepsilon_l})$ so that the $\mathcal{O}(1)$ equation (in the inner layer) for the pollutant transport gives

$$[\hat{u}_- - \hat{R}_s \xi'_s(\tau)] \frac{\partial c_0}{\partial \bar{x}} = 0$$

and since $\frac{\partial c_0}{\partial \bar{x}} \neq 0$, we have $\xi'_s(\tau) = \frac{\hat{u}_-}{\hat{R}_s}$ which determines the shock position, i.e., $\xi_s(\tau) = \hat{u}_- \tau / \hat{R}_s$ satisfying $\xi(0) = 0$. This solution agrees with the shock position obtained from the outer solution, see (29). Analysis of the first order terms gives the solution in the inner layer. Applying the boundary conditions we have

$$\hat{s}(x, t) = \frac{\mathcal{A}_s}{2} - \frac{\mathcal{A}_s}{2} \operatorname{erf} \left(\frac{x - \hat{u}_- t / \hat{R}_s}{\sqrt{\varepsilon_l}} \sqrt{\frac{\hat{R}_s}{4t}} \right),$$

which is the leading order approximate solution for the substrate equation. A similar analysis of the equation governing the acceptor concentration gives the shock location at $\xi_a(\tau) = \hat{u}_- \tau$. Similarly, for the nutrient we have

$$\hat{a}(x, t) = \frac{\mathcal{A}_a}{2} - \frac{\mathcal{A}_a}{2} \operatorname{erf} \left(\frac{x - \hat{u}_- t}{\sqrt{\varepsilon_l}} \sqrt{\frac{1}{4t}} \right),$$

where $\mathcal{A}_a = 1 - \sqrt{\varepsilon_l} \frac{\alpha \lambda_2 x}{\hat{u}_- \kappa_a + 1} \frac{1}{\kappa_s + 1}$.

Consider the equation governing the decay and production of biomass. The solution $\hat{m}(\bar{x}, \tau)$ follows from the approximate solutions $\hat{s}(\bar{x}, \tau)$ and $\hat{a}(\bar{x}, \tau)$. In the inner region we have:

$$\frac{\partial \eta}{\partial \tau} - \frac{\xi_m(\tau)}{\sqrt{\varepsilon_l}} \frac{\partial \eta}{\partial \bar{x}} = -\alpha \lambda_4 \sqrt{\varepsilon_l} (\eta - 1) + \alpha \lambda_3 \sqrt{\varepsilon_l} \hat{m} \frac{c}{\kappa_s + c} \frac{g}{\kappa_a + g}. \tag{33}$$

We seek a solution to (33) in the form $\eta(\bar{x}, \tau) = \eta_0(\bar{x}, \tau) + \sqrt{\varepsilon_l} \eta_1(\bar{x}, \tau) + \dots$ for $c(\bar{x}, \tau) \sim c_0(\bar{x}, \tau)$ and $g(\bar{x}, \tau) \sim g_0(\bar{x}, \tau)$. The $\mathcal{O}(1)$ expansion gives $\xi_m(\tau) = 0$, since $\frac{\partial \eta}{\partial \bar{x}} \neq 0$, satisfying the initial condition $\xi_m(0) = 0$. The $\mathcal{O}(\sqrt{\varepsilon_l})$ expansion gives

$$\frac{\partial \eta_0}{\partial \tau} = 0.$$

Using the initial condition $\eta_0(\bar{x}, 0) = 1$ we have, at leading order, $\eta_0(\bar{x}, \tau) = 1$. The $\mathcal{O}(\varepsilon_l)$ terms are

$$\frac{\partial \eta_1}{\partial \tau} = -\alpha \lambda_4 (\eta_0 - 1) + \alpha \lambda_3 \eta_0 \frac{c_0}{\kappa_s + c_0} \frac{g_0}{\kappa_a + g_0}.$$

But $\eta_0(\bar{x}, \tau) = 1$ and $c_0(\bar{x}, \tau)$ and $g_0(\bar{x}, \tau)$ are given above, so we have

$$\frac{\partial \eta_1}{\partial \tau} = \alpha \lambda_3 \eta_0 \frac{c_0}{\kappa_s + c_0} \frac{g_0}{\kappa_a + g_0},$$

where $\bar{x} \in (-\infty, \infty)$. Integrating gives:

$$\eta_1 = \int_0^\tau \alpha \lambda_3 \eta_0 \frac{c_0}{\kappa_s + c_0} \frac{g_0}{\kappa_a + g_0} d\tau,$$

i.e.,

$$\hat{m} = 1 + \sqrt{\varepsilon_l} \alpha \lambda_3 \int_0^t \frac{\hat{s}}{\kappa_s + \hat{s}} \frac{\hat{a}}{\kappa_a + \hat{a}} dt.$$

To verify these results we use the numerical method of lines. This involves discretizing the equations in space to obtain a set of ordinary differential equations which are then integrated using MATLAB routine `ode15s`. For all the simulations we set both the relative and absolute error tolerance to 10^{-6} .

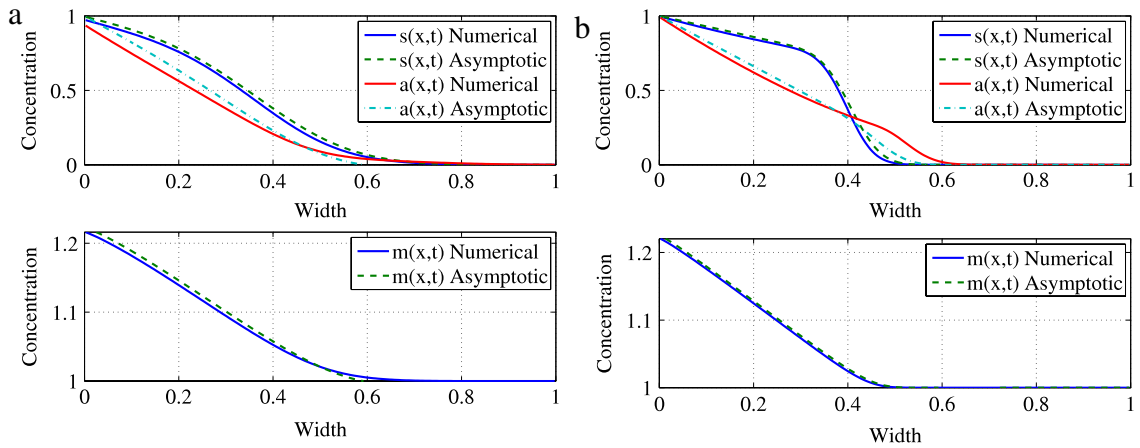


Fig. 4. Comparison of the numerical solution and the approximate solution for (a) $\epsilon_l = 0.015$ and $t = 1.0$, (b) $\epsilon_l = 0.0015$ and $t = 0.7$.

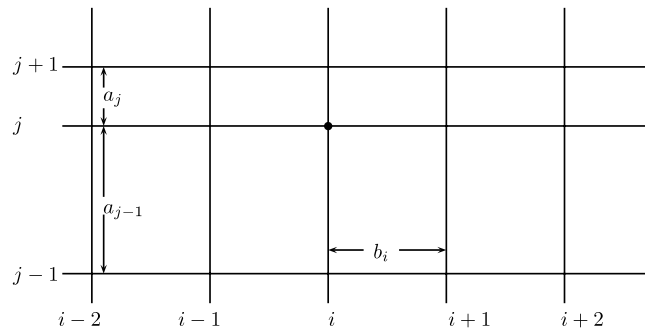


Fig. 5. Inner nodes system.

4.1.7. Sensitivity to ϵ_l

To demonstrate the accuracy of the numerical solution, in Fig. 4 we plot the asymptotic solution and numerical solution for a fixed value of t and different values of ϵ_l . In general, the two solutions are so close that their fronts are indistinguishable for $\epsilon_l = 0.0015$. The sharpening of the shock layer as ϵ_l decreases is also evident.

In Appendix, we show how the effects of small pore clogging on the flow field can be investigated.

5. The full model

Finite difference and finite elements methods have been used in many problems involving free or moving boundaries [3,27]. Chapwanya and O’Brien [3] used a trial free boundary method to predict the position of a free surface. This method is based on making an initial guess at the position of the free boundary, $\Gamma^{(k)}$ say. Then an approximation for the pressure field inside the saturated porous domain is computed using the given conditions for the ‘fixed’ boundaries together with one of the two conditions on the free boundary. The improved free boundary position $\Gamma^{(k+1)}$ is found by demanding that the remaining free boundary condition is satisfied. The process is terminated when all the Γ s agree to a given degree of accuracy.

In the present study, both explicit and implicit finite difference methods are used to simultaneously compute the position of the moving boundary and the concentration profiles. The discretized finite difference expressions will allow for a non-uniform grid space in all the directions. The corresponding nodal discretization is shown in Fig. 5 which leads to a modification of the derivatives in the governing equations. Introducing the Lagrangian formulation requires

$$\frac{d}{dt} = \frac{\partial}{\partial t} + \dot{y} \frac{\partial}{\partial y} + \dot{x} \frac{\partial}{\partial x}, \tag{34}$$

to describes the change while moving along the space coordinate. The dot denotes a derivative with respect to time. We discretize the equations by replacing the space derivatives as follows; for the non-uniform grid we have

$$\frac{\partial}{\partial y} \left(\theta \frac{\partial s}{\partial y} \right) \approx \frac{1}{a_{j-1/2}} \left\{ \theta_{i,j+1/2} \frac{s_{i,j+1} - s_{i,j}}{a_j} - \theta_{i,j-1/2} \frac{s_{i,j} - s_{i,j-1}}{a_{j-1}} \right\}, \tag{35}$$

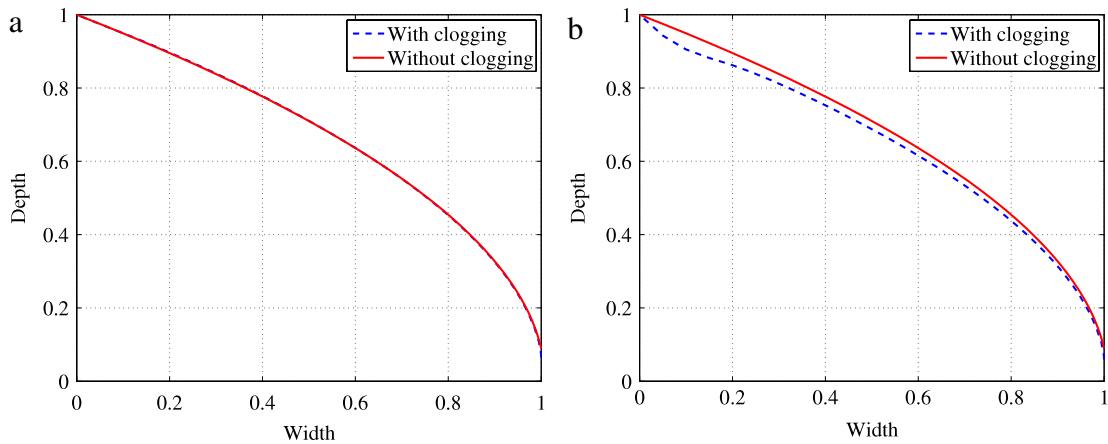


Fig. 6. (a) The moving boundary position at $t = 1.0$. (b) The moving boundary position at $t = 10$.

Table 1

Selected input data for the simulations.

Symbol	Description	Value	Units	Reference
K_s	Hydrocarbon saturation constant	2.00	g/m ³	[16]
K_a	Oxygen saturation constant	1.00	g/m ³	[16]
m_0	Background biomass concentration	12.8	g/m ³	[8]
s_0	Influent hydrocarbon concentration	26.0	g/m ³	[16]
a_0	Influent oxygen concentration	16.5	g/m ³	[16]
b	Microbial decay constant	0.10	1/day	[22]
k_m	Utilization constant	1.20	1/day	[16]
D_l	Longitudinal diffusion constant	0.25	m ² /day	[16]
D_t	Transverse diffusion constant	0.25	m ² /day	[16]
ρ_m	Biomass density	2.5×10^3	g/m ³	[8]
ρ_ℓ	Liquid water density	1.0×10^6	g/m ³	[20]
ρ_b	Bulk aquifer density	1.60×10^6	g/m ³	[8]
μ_ℓ	Dynamic viscosity	8.64×10^4	g/day/m	[20]
k_0	Permeability	2.00×10^{-11}	m ²	[20]
Y	Microbial yield coefficient	0.50	-	[16]
ϕ	Porosity	0.39	-	[8]
X	Stoichiometric constant	2.40	-	[16]
Dimensionless parameters:				
A		0.208		
λ_1		0.407		Eq. (12)
λ_2		2.400		Eq. (12)
λ_3		0.645		Eq. (12)
λ_4		0.645		Eq. (12)
χ	Biomass ratio	0.0051		
ε_l	Longitudinal diffusivity	0.0015		Eq. (12)
ε_t	Transverse diffusivity	0.0066		Eq. (12)
δ^2	Aspect ratio	0.051		Section 2

where $a_{j-1} = y_j - y_{j-1}$, $a_{j-1/2} = (a_j + a_{j-1})/2$, $\theta_{j+1/2} = (\theta_j + \theta_{j+1})/2$ and $\theta_{j-1/2} = (\theta_j + \theta_{j-1})/2$. For the first derivatives we apply a three-point backward formula

$$\frac{\partial(u\theta s)}{\partial x} \approx \frac{3[u\theta s]_{i,j} - 4[u\theta s]_{i-1,j} + [u\theta s]_{i-2,j}}{b_{i-1} + b_{i-2}} \tag{36}$$

The other partial derivatives are discretized in the same way. The resulting semi-discretization is fully second order accurate in space and leads to a system of ordinary differential equations for the discrete solution values which we then integrate in time using Matlabs stiff solver ODE15s. We set both relative and absolute error tolerances for ODE15s to 10^{-8} .

5.1. Simulations

Fig. 7 gives the profiles for the velocity, pollutant concentration, nutrient concentration, biomass concentration and the concentration history at a point $x = 0.10$ and $y = 0.42$. In all the figures, we use the parameter values given in Table 1.

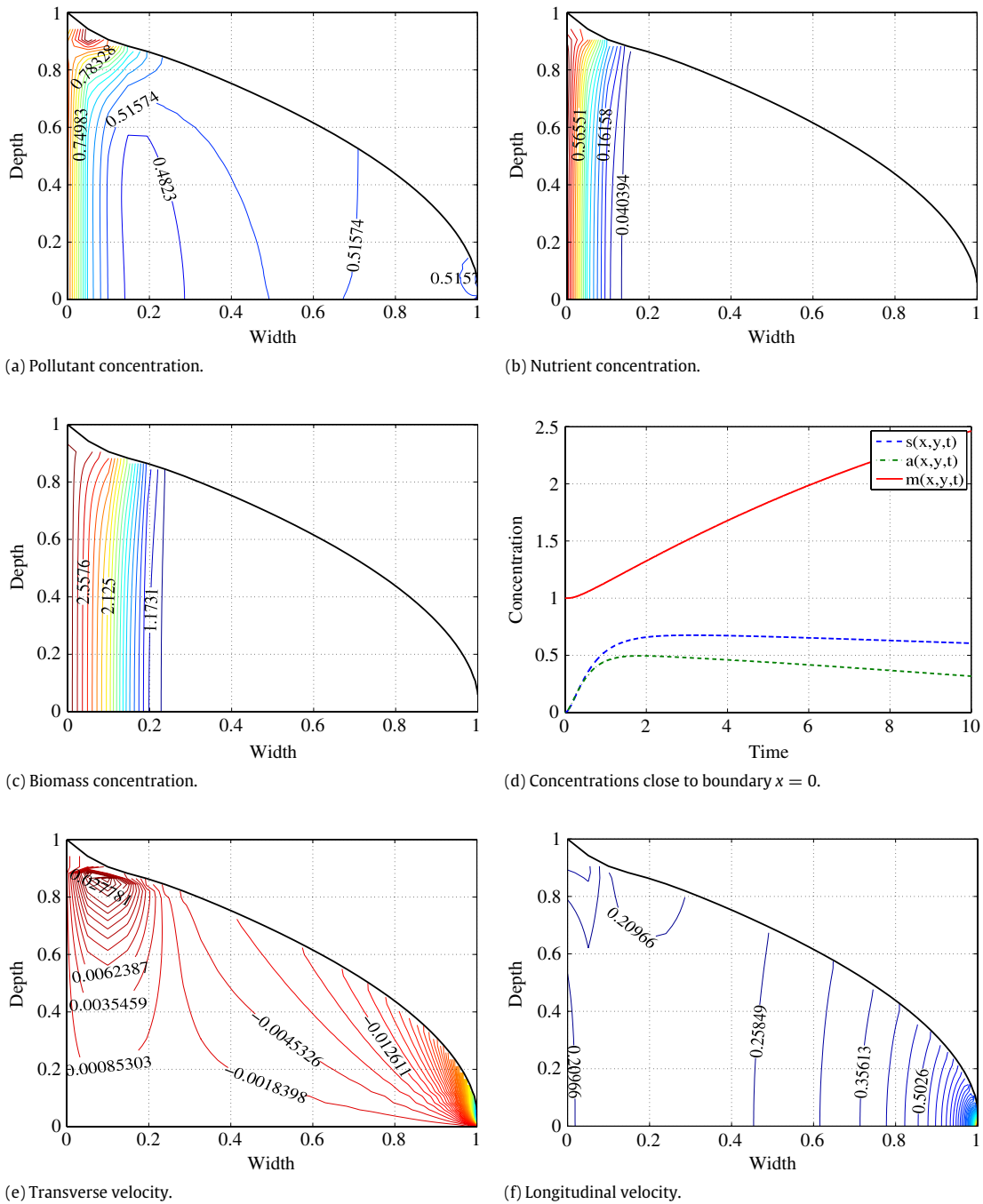


Fig. 7. All the profiles were taken at $t = 10$. In (d), the concentrations were taken at the point $(x = 0.1, y = 0.5)$.

In Fig. 6, we show simulations for the moving boundary position at two different time intervals. There is a significant increase in biomass concentration in the regions where the nutrient and pollutant concentrations overlap, see Fig. 7. This has the direct effect of decreasing the height of the phreatic surface which is consistent with the predictions from the approximate one dimensional solution, see Appendix.

6. Conclusions and future work

We have considered a model for bioremediation applied to the seepage of pollutants through an earth wall. The model involves a full coupling of the fluid velocity and the degradation process. As opposed to idealized situations in the literature,

the current model is solved for field flow conditions. The numerical solution is validated by obtaining an approximate solution in the limit of low background biomass concentration. The bio-clogging phenomenon, as given by the correction terms, suggests a lowering of the moving boundary position and a decrease in the solute injection concentrations.

Studies of steady state flow problems of seepage through earth walls are available in the literature, see for example [21]. Such problems may be solved, to a reasonable degree of accuracy, by the Dupuit approximation. However, in the present formulation the Dupuit approximation fails to predict the seepage face height which is an integral part of the physical application of the model. Thus we have presented a numerical strategy which computes the seepage face and the position of the moving boundary. We note that the correction terms predict no change in the seepage height, see boundary conditions to Eq. (48) and the two dimensional simulations.

The equations being solved are complex and the approximate solution involved a double expansion for $\chi \ll 1$ and $\varepsilon_l \ll 1$ in the distinguished limit, $\delta^2 = \sqrt{\varepsilon_l}$. This model and solution strategy can clearly be extended to more general systems including more nutrient and biomass species as well both fully two- and three dimensional aquifers.

Acknowledgements

This work was supported by grants from the Natural Sciences and Engineering Research Council of Canada and the MITACS Network of Centres of Excellence. SOB acknowledges the support of the Mathematics Applications Consortium for Science and Industry (www.macci.ul.ie) funded by the Science Foundation Ireland mathematics initiative grant 06/MI/005.

Appendix

A.1. The effect of nonzero $\mathcal{O}(\chi)$ on the flow

In Section 4.1 we computed the leading order solution for flow in the form

$$\hat{p} = \hat{h} - y, \quad \hat{u} \approx -\frac{\partial \hat{h}}{\partial x}, \quad \hat{v} \approx \sqrt{\varepsilon_l y} \frac{\partial^2 \hat{h}}{\partial x^2},$$

where $\hat{h} = \hat{h}(x)$, $\hat{s} = \hat{s}(x, t)$, $\hat{a} = \hat{a}(x, t)$ and $\hat{m} = \hat{m}(x, t)$ are all known. Here we investigate the effect of small pore clogging on the flow by seeking expansions of the form $c \sim \hat{c} + \chi \hat{c}_2$. The $\mathcal{O}(\chi)$ equation governing the correction to the pressure field is given by

$$\sqrt{\varepsilon_l} \frac{\partial^2 \hat{p}_1}{\partial x^2} + \frac{\partial^2 \hat{p}_1}{\partial y^2} = \sqrt{\varepsilon_l} \kappa \frac{\partial}{\partial x} \left(\hat{m} \frac{\partial \hat{h}}{\partial x} \right) - \sqrt{\varepsilon_l} \frac{\partial \hat{m}}{\partial t}, \tag{37}$$

with the following boundary conditions

$$\frac{\partial \hat{p}_1}{\partial y} = 0, \quad \text{on } y = 0, \tag{38}$$

$$\hat{p}_1 - \hat{h}_1 = 0, \quad \sqrt{\varepsilon_l} \frac{\partial \hat{h}_1}{\partial t} = -\frac{\partial \hat{p}_1}{\partial y} + \sqrt{\varepsilon_l} \frac{\partial \hat{h}}{\partial x} \left[\frac{\partial \hat{p}_1}{\partial y} + \frac{\partial \hat{h}_1}{\partial x} - \frac{\partial \hat{h}}{\partial x} \kappa \hat{m} \right], \quad \text{on } y = \hat{h}, \tag{39}$$

$$\hat{p}_1 = 0, \quad \text{on } x = 0, \tag{40}$$

$$\hat{p}_1 = 0, \quad \text{on } x = 1. \tag{41}$$

The corresponding $\mathcal{O}(\chi)$ biodegradation equations are given by

$$\hat{R}_s \frac{\partial \hat{s}_1}{\partial t} = -\hat{u} \frac{\partial \hat{s}_1}{\partial x} + \varepsilon_l \frac{\partial^2 \hat{s}_1}{\partial x^2} + F_s(x, t) - \lambda_1 \Gamma_m(x, t) \tag{42}$$

$$\frac{\partial \hat{a}_1}{\partial t} = -\hat{u} \frac{\partial \hat{a}_1}{\partial x} + \varepsilon_l \frac{\partial^2 \hat{a}_1}{\partial x^2} + F_a(x, t) - \lambda_1 \lambda_2 \Gamma_m(x, t) \tag{43}$$

$$\frac{\partial \hat{m}_1}{\partial t} = -\lambda_1 \lambda_4 \hat{m}_1 + \lambda_1 \lambda_3 \Gamma_m(x, t), \tag{44}$$

where

$$F_s(x, t) = \hat{R}_s \hat{s} \frac{\partial \hat{m}}{\partial t} - \hat{R}_{s1} \frac{\partial \hat{s}}{\partial t} - \hat{u}_1 \frac{\partial \hat{s}}{\partial x} - \varepsilon_l \frac{\partial \hat{m}}{\partial x} \frac{\partial \hat{s}}{\partial x},$$

$$F_a(x, t) = \hat{a} \frac{\partial \hat{m}}{\partial t} - \hat{u}_1 \frac{\partial \hat{a}}{\partial x} - \varepsilon_l \frac{\partial \hat{m}}{\partial x} \frac{\partial \hat{a}}{\partial x},$$

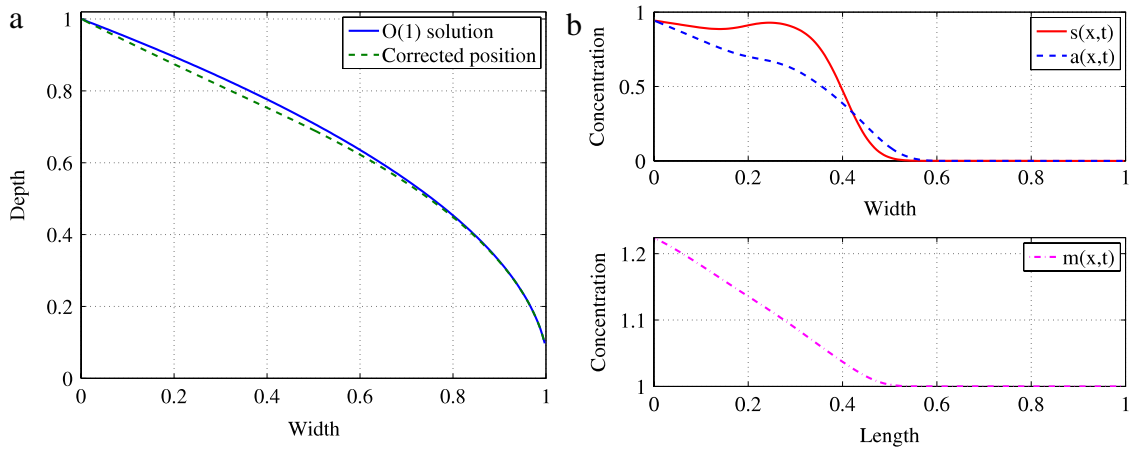


Fig. 8. (a) The corrected moving boundary position at $t = 1.0$. (b) The corrected concentration profiles at $t = 1.0$ for $\varepsilon_l = 0.0015$. In both figures we adjust χ to 0.1 to highlight the effects of clogging.

and

$$\Gamma_m(x, t) = \frac{\hat{m}\hat{s}_1 + (\hat{m}\hat{a}_1 + \hat{m}_1\hat{a})\hat{s}}{(\kappa_a + \hat{a})(\kappa_s + \hat{s})} - \frac{\hat{m}\hat{a}\hat{s}_1}{(\kappa_s + \hat{s})(\kappa_a + \hat{a})^2} - \frac{\hat{m}\hat{a}\hat{s}\hat{s}_1}{(\kappa_s + \hat{s})^2(\kappa_a + \hat{a})},$$

and $\hat{R}_{s1} = \hat{A}\hat{m}$ where $\hat{s}(x, t)$, $\hat{a}(x, t)$ and $\hat{m}(x, t)$ are the known leading order solutions obtained for $\sqrt{\varepsilon_l} \ll 1$. The boundary conditions at $x = 0$ are

$$\varepsilon_l \frac{\partial \hat{s}_1}{\partial x} = \hat{u}\hat{s}_1 + \hat{u}_1(\hat{s} - 1), \quad \varepsilon_l \frac{\partial \hat{a}_1}{\partial x} = \hat{u}\hat{a}_1 + \hat{u}_1(\hat{a} - 1),$$

with the initial conditions

$$\hat{s}_1(x, 0) = 0, \quad \hat{a}_1(x, 0) = 0, \quad \hat{m}_1(x, 0) = 0.$$

To complete the model, the velocity components are

$$\hat{u}_1 = -\frac{\partial \hat{p}_1}{\partial x} + \kappa \hat{m} \frac{\partial \hat{h}}{\partial x}, \quad v_1 = -\frac{\partial \hat{p}_1}{\partial y}. \tag{45}$$

where $\kappa = 19/6$. Similar to the approach at leading order, we only need to solve for the moving boundary correction to find a correction to the flow velocity. Note that the moving boundary correction is now time dependent.

A.2. Solutions

Using the distinguished limit $\delta^2 = \sqrt{\varepsilon_l}$ we seek a solution for the pressure in the form

$$\hat{p}_1 = \varphi_0 + \sqrt{\varepsilon_l}\varphi_1 + \mathcal{O}(\sqrt{\varepsilon_l}).$$

From Eq. (37), we have

$$\frac{\partial^2 \varphi_0}{\partial y^2} = 0,$$

which can be integrated to give

$$\varphi_0 = \hat{h}_1, \tag{46}$$

satisfying the boundary condition $\varphi_0(x, h_0) = \hat{h}_1$ and $\frac{\partial \varphi_0}{\partial y}(x, 0) = 0$. The $\mathcal{O}(\sqrt{\varepsilon_l})$ terms in (37) give

$$\frac{\partial^2 \varphi_0}{\partial x^2} + \frac{\partial^2 \varphi_1}{\partial y^2} = \kappa \frac{\partial}{\partial x} \left(\hat{m} \frac{\partial \hat{h}}{\partial x} \right) - \frac{\partial \hat{m}}{\partial t},$$

which can be simplified to yield

$$\frac{\partial^2 \varphi_1}{\partial y^2} = \kappa \frac{\partial}{\partial x} \left(\hat{m} \frac{\partial \hat{h}}{\partial x} \right) - \frac{\partial \hat{m}}{\partial t} - \frac{\partial^2 \hat{h}_1}{\partial x^2}. \tag{47}$$

Integrating (47) together with the boundary conditions leads to

$$\frac{\partial \hat{h}_1}{\partial t} = -\hat{h} \left[\kappa \frac{\partial}{\partial x} \left(\hat{m} \frac{\partial \hat{h}}{\partial x} \right) - \frac{\partial \hat{m}}{\partial t} - \frac{\partial^2 \hat{h}_1}{\partial x^2} \right] + \frac{\partial \hat{h}}{\partial x} \left[\frac{\partial \hat{h}_1}{\partial x} - \frac{\partial \hat{h}}{\partial x} \kappa \hat{m} \right]. \quad (48)$$

The boundary conditions to (48) come from (40) and (41), i.e.,

$$\hat{h}_1(0, t) = \hat{h}_1(1, t) = 0.$$

To complete the analysis, we find a numerical solution to Eqs. (42), (43), (44) and (48). In particular, Eq. (48) gives a correction to the position of the moving boundary in the presence of growing biomass population. Eq. (46) completes the solution.

The $\mathcal{O}(\chi)$ equations together with the leading order solution give the approximate solution to (9)–(11) in the form $s(x, t) \approx \hat{s} + \chi \hat{s}_1$, $a(x, t) \approx \hat{a} + \chi \hat{a}_1$, and $m(x, t) \approx \hat{m} + \chi \hat{m}_1$. Interestingly, this (crude) model predicts a decrease in the height of the phreatic surface as biomass concentration increases since less water flows into the domain. This phenomenon is evident in Fig. 8 where there is a significant decrease in pollutant and nutrient concentration at the inflow boundary. Note that for $\chi = 0.0051$, the corrected boundary position and the leading order solution are indistinguishable. Thus, for illustrative purposes, Fig. 8 is shown for $\chi = 0.051$.

References

- [1] H.V. Nguyen, J.L. Nieber, P. Odoro, L.W. Dekker, T.S. Steenhuis, Modelling solute transport in a water repellent soil, *J. Hydrol.* 215 (1999) 188–201.
- [2] S.M. Hassanizadeh, M.A. Celia, H.K. Dahle, Dynamic effect in the capillary pressure-saturation relationship and its impact on unsaturated flow, *Vadose Zone J.* 1 (2002) 38–57.
- [3] M. Chapwanya, S.B.G. O'Brien, Corner and start-up singularities in porous flow, *J. Comput. Appl. Math.* 176 (1) (2005) 163–177.
- [4] K.T.B. MacQuarrie, E.A. Sudicky, E.O. Frind, Simulation of biodegradable organic contaminants in groundwater: 1. Numerical formulation in principal directions, *Water Resour. Res.* 26 (2) (1990) 207–222.
- [5] F.J. Molz, M.A. Widdowson, L.D. Benefield, Simulation of microbial growth dynamics coupled to nutrient and oxygen transport in porous media, *Water Resour. Res.* 22 (8) (1986) 1207–1216.
- [6] W.S. Dockins, G.J. Olson, G.A. McFeters, S.C. Turbak, Dissimilatory bacterial sulphate reduction in Montana groundwaters, *Geomicrobiol. J.* 2 (1980) 83–98.
- [7] R.C. Borden, P.B. Bedient, Transport of dissolved hydrocarbons influenced by oxygen-limited biodegradation 1. Theoretical development, *Water Resour. Res.* 22 (13) (1986) 1973–1982.
- [8] J. Kildsgaard, P. Engesgaard, Numerical analysis of biological clogging in two dimensional sand box experiments, *J. Contam. Hydrol.* 50 (2001) 261–285.
- [9] S.K. Tiwari, K.L. Bowers, Modeling biofilm growth for a porous media applications, *Math. Comput. Modelling* 33 (2001) 299–319.
- [10] B. Chen, Y. Li, Simulation of thick biofilm growth at the microscale, *Appl. Numer. Math.* 40 (2002) 261–271.
- [11] H.J. Dupin, P.L. McCarty, Impact of colony morphologies and disinfection on biological clogging in porous media, *Environ. Sci. Technol.* 34 (2000) 1513–1520.
- [12] M. Thullner, L. Maucilaire, M.H. Schroth, J. Zeyer, W. Kinzelbach, Interaction between water flow and spartial distribution of microbial growth in a two-dimensional flow field in saturated porous media, *J. Contam. Hydrol.* 58 (2002) 169–189.
- [13] S. Chawla, S.M. Lenhart, Application of optimal control to bioremediation, *J. Comput. Appl. Math.* 114 (2000) 81–102.
- [14] M. Thullner, M.H. Schroth, J. Zeyer, W. Kinzelbach, Modeling of a microbial growth experiment with bioclogging in a two-dimensional saturated porous media flow field, *J. Contam. Hydrol.* 70 (2004) 37–62.
- [15] R. Murray, J.X. Xin, Existence of traveling waves in a biodegradation model for organic contaminants, *SIAM J. Math. Anal.* 30 (1) (1998) 72–94.
- [16] L. Semprini, P.L. McCarty, Comparison between simulations and field results for in-situ bioremediation of chlorinated aliphatics: Part 1. Biostimulation of methanotrophic bacteria, *Ground Water* 29 (3) (1991) 365–374.
- [17] T.P. Clement, B.S. Hooker, R.S. Skeen, Macroscopic models for predicting changes in saturated porous medium properties caused by microbial growth, *Ground Water* 34 (5) (1996) 934–942.
- [18] J. Bear, *Hydraulics of Groundwater*, in: McGraw-Hill Series in Water Resources and Environmental Engineering, New York, 1979.
- [19] G. Keady, A Dupuit approximation for the rectangular dam problem, *IMA J. Appl. Math.* 44 (1990) 243–260.
- [20] A.C. Fowler, *Mathematical Models in the Applied Sciences*, Cambridge University Press, 1997.
- [21] J.H. Knight, Improving the Dupuit–Forchheimer groundwater free surface approximation, *Adv. Water Res.* 28 (2005) 1048–1056.
- [22] S. Oya, A.J. Valocchi, Analytical approximation of biodegradation rate for in situ bioremediation of groundwater under ideal radial flow conditions, *J. Contam. Hydrol.* 31 (1998) 275–293.
- [23] S.W. Taylor, P.R. Jeffé, Substrate and biomass transport in a porous medium, *Water Resour. Res.* 26 (9) (1990) 2181–2194.
- [24] S.N. Maurya, A.K. Mittal, Applicability of equilibrium isotherm models for the biosorptive uptakes in comparison to activated carbon-based adsorption, *J. Environ. Eng.* 132 (12) (2006) 1589–1599.
- [25] R.S. Johnson, *A Morden Introduction to the Mathematical Theory of Water Waves*, Cambridge University Press, 1997.
- [26] S.B.G. O'Brien, M.A. Hayes, A model for gravity driven flow of a thin liquid solid suspension with evaporation effects, *Z. Math. Phys.* 56 (2005) 1–22.
- [27] J. Crank, *Free and Moving Boundary Problems*, Oxford University Press Inc., New York, 1984.